Simulation of Lubricant Recovery After Heat Assisted Magnetic Recording Writing

Joanna Bechtel Dahl

David B. Bogy

June 21, 2013

Abstract

The lubricant in a heat assisted magnetic recording (HAMR) hard disk drive must be able to withstand the writing process in which the disk is locally heated a few hundred degrees Celsius within a few nanoseconds and be able to sufficiently recover the lubricant depletion and accumulation zones so as to allow for stable flying heights and reliable read/write performance. In a previous publication, we simulated the distortion of thin Zdol films due to a thermal spot during HAMR writing and predicted several Angstroms of depletion. In this paper, we continue these simulations into recovery. Our simulation results indicate that lubricant deformation caused by small thermal spots of 20 nm full-width half maximum (FWHM) recover on the order of 100–1000 times faster than larger 1 μm FWHM spots. However, the lubricant is unable to recover from sufficiently high writing temperatures. An optimal thickness at which HAMR writing deformation recovers fastest is apparent for sub-100 nm FWHM thermal spots. Our simulations show that simple scaling of experimental observations using optical laser spots of diameters close to 1 μm to predict lubricant phenomena induced by thermal spots close to 20 nm FWHM may not be valid. Researchers should be aware of the possibility of different lubricant behavior at small scales when designing and developing the HAMR head-disk interface.

1 Introduction

The magnetic recording industry widely views heat assisted magnetic recording (HAMR) as a technology to achieve storage densities beyond 1 Tb/in^2 in hard disk drives [31, 14, 1]. Continued development of the tribological design of the head-disk interface (HDI) is required along with advancements of other HAMR system components in order to maintain the mechanical reliability of the head/disk interface despite decreased spacing and adverse thermal conditions. One critical component of the HDI is the lubricant coating on the magnetic disk that protects the disk and recording head from damage due to intermittent contacts during normal drive operations. The HAMR lubricant must be able to withstand the writing process in which the disk is locally heated

a few hundred degrees Celsius within a few nanoseconds to reduce the coercivity of the media and allow writing of data. In addition, the lubricant must be able to recover the depletion and accumulation zones induced by HAMR writing so as to allow for stable flying heights and reliable read/write performance. In a previous publication, we simulated the distortion of thin Zdol films due to a thermal spot during HAMR writing and predicted several Angstroms of depletion in some cases [4]. In particular, for a 20 nm FHWM thermal spot reaching a maximum temperature of 350°C , systems of thickness greater than 1 nm show possibly significant peak-to-peak deformation ranging from 3.0–5.6 Å . In this paper, we continue these simulations into recovery to evaluate HAMR system factors that can lead to poor HDI performance.

Perfluoropolyethers (PFPEs) are common lubricants used in the magnetic recording industry due to their favorable properties that enable them to reduce wear and friction at conventional hard drive operating temperatures throughout the drive lifetime. Lubricant properties can be further improved and customized by adding functional end-groups, such as the hydroxyl end-groups on difunctional Zdol and tetrafunctional Ztetrol molecules that interact with the amorphous carbon overcoat through hydrogen bonding [33]. The addition of mid-chain functional groups has resulted in improved minimum clearance and evaporation properties [8]. Because of Zdol's long history in the hard drive industry and widespread use in products in the 1990s, there is much published experimental data and theoretical analysis on which to base Zdol property models in our simulation tool. So while Zdol is not in common use today, as a first step in predicting HAMR lube behavior, we will analyze this conventional lubricant.

Experimental studies of lubricant recovery suggest that the lubricant depletion zone due to HAMR writing may not recover by the next laser pass in approximately 6–15 ms, the time for one disk revolution in 10,000–4000 RPM drives, at least for the laser spot sizes used in the experiments. Though their experiments involved scanning a laser back and forth, not a single laser pass as we simulate, Ma et al. [21, Figure 3] show a significant trough of depth 0.8 nm for an initially 1.2 nm thick functionalized lubricant 5 minutes after laser illumination. In a similar paper, the authors report 0.5 nm of peak-to-peak lubricant depletion is relaxed to less than 0.1 nm trough depth after a long 5 hours of recovery [20, Figure 2]. Though not the same initial deformation as following HAMR writing, the free surface spreading of PFPE lubricants relaxing from a sharp stair-step interface show significant changes after several minutes of spreading [13, 19]. Thus the several Angstrom deep troughs in HAMR lubricants after writing could be present for subsequent laser passes in the immediately following disk revolutions.

A large amount of lubricant deformation can compromise the mechanical stability of the HDI through slider flying modulations or lubricant loss [7, 6] and lead to poor read/write efficiency. In one particular experimental study, drops introduced on the disk surface of height 10–20 Å and lateral dimensions 50–100 μm caused up to 100 nm of slider flying height increase over the first 10 revolutions before the slider gradually removed the lubricant drop obstacle [29]. Though the amplitude was only 2–3 Å height, periodic ripples induced large slider flying height modulations via a resonant effect on slider dynamics, with a peak flying height modulation of 0.8 nm (mean to peak) which resulted in a large flying height loss of $\sim$2 nm with 3σ [5]. Few experimental studies addressing slider-lubricant interactions for HAMR systems have been published [9], but we conjecture that HAMR writing lubricant deformation that results in large

obstacles or periodic disturbances is undesirable.

Numerical studies of lubricant recovery based on continuum lubrication theory have been conducted for conventional (non-HAMR) hard drive systems. Early lubricant recovery flow simulations using a constant viscosity indicate that the time scale for the initially 5 nm thick lubricant to replenish a 100 μm-wide, 3 nm deep trough is several minutes [25]. Ma et al. [18] numerically investigate the effect of functional end-groups, molecular weight, and carbon overcoat on lubricant recovery into a 1 μm diameter hole with the diffusion equation; the authors use experimental data from the spreading of a sharp stair-step lubricant interface to determine the diffusion coefficient thickness dependence and predict critical reflow time. While several authors have simulated lubricant flow and evaporation under HAMR writing conditions [38, 39, 22], to our knowledge simulations of recovery of the trough and side ridges after HAMR writing have yet to be published in the literature.

In this paper we modify our simulation tool from our previous HAMR writing publication [4] to simulate Zdol lubricant recovery on the disk surface following HAMR writing. First we describe our continuum lubricant model that includes the film thickness dependencies of viscosity and dispersive and polar contributions to disjoining pressure. We present recovery simulation results for length and time scales unobservable with current experimental capabilities: laser spot sizes less than 1 μm and lubricant recovery in the first few microseconds after laser illumination. We investigate how initial thickness, thermal spot size during HAMR writing, and thermal spot maximum temperature affect Zdol lubricant recovery after HAMR writing.

2 Lubricant Model

2.1 Governing Evolution Equation

Lubrication theory based on continuum mechanics exploits the difference in length scales between the film thickness direction and the planar directions. In our case, the characteristic film thickness h_0 is close to 1 nm. This is much smaller than the slider length ($\sim$ 800 μm) and at least an order of magnitude smaller than the expected laser FWHM used in HAMR ($\sim$ 25 nm for ultra high density HAMR recording of 5 Tb/in^2 [1]). Thus the key requirement of lubrication theory is satisfied in our system. We are obviously pushing the limits of continuum theory by using lubrication theory to describe the HAMR lubricant. However, other researchers have found that continuum theory can be an adequate approach for predicting PFPE lubricant flow on a hard drive disk even as the thickness approaches one monolayer [24, 32, 23]. Thus we will use the lubrication theory approach as a starting point for studying lubricant recovery after HAMR writing. However, keep in mind several limitations of lubrication theory for modeling this Zdol system. No information about the microstructure and particular polymer conformation is provided by continuum theory, factors that may be important in monolayer functional lubricants not illuminated by the continuum behavior studies mentioned above. Our simulations are only as good as the constitutive law (stress-strain relationship) used, parameters for which are inferred from experiments.

In our application of the lubrication approximation, shown in Figure 1, the viscous

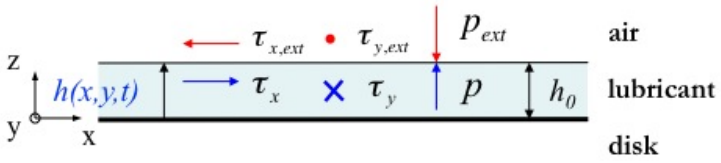

Figure 1: HAMR lubricant recovery process schematic: The thin lubricant film of unknown thickness $h(x,y,t)$ has been subjected to a scanning thermal spot and resulted in a depletion zone and possibly accumulation in side ridges. Lubricant reflow is driven by the pressure gradient ∇p_{ext} due to Laplace pressure and disjoining pressure.

liquid is bounded below by a horizontal solid substrate (the magnetic recording disk) and above by an interface between the liquid film and a passive gas (the air bearing). In this problem, the lubricant film thickness $h(x,y,t)$ is unknown and the unknown lubricant pressure $p(x,y,t)$ is a functional of h via the surface tension and disjoining pressure. PFPE lubricants exhibit viscoelastic behavior [10], but here we retain the purely viscous model. The incorporation of a viscoelastic constitutive model into our HAMR lubricant simulations will be the subject of a future report.

We choose a coordinate system fixed to the spinning disk, so the advective effects are not needed in the governing equation. The final governing evolution equation for our HAMR lubricant system under recovery conditions is:

$$\frac{\partial h}{\partial t} + \frac{\partial}{\partial x}\left(-\frac{h^3}{3\eta}\frac{\partial p}{\partial x} + \frac{h^2}{2\eta}\tau_x\right) + \frac{\partial}{\partial y}\left(-\frac{h^3}{3\eta}\frac{\partial p}{\partial y} + \frac{h^2}{2\eta}\tau_y\right) = 0, \tag{1}$$

where h is the unknown lubricant thickness, η is the lubricant viscosity, p is the lubricant pressure, τ_x is the lubricant shear stress in the x direction (down-track), τ_y is the lubricant shear stress in the y direction (cross-track), and ρ is the constant lubricant density. A rigorous derivation of this governing evolution equation is presented in [27]. The lubricant pressure and shear stress are determined by a force balance at the lubricant-air interface. In these simulation we do not include the air bearing pressure, air shearing stresses or centripetal acceleration. Those effects are also left to the subject of another lubricant study.

The disk is assumed to have instantaneously cooled to ambient temperature once the laser is turned off. We infer from previous simulation and experimental results that for HAMR lubricant recovery simulations, transient disk temperature effects are limited to the first 100 ns of simulation and therefore an instantaneously ambient temperature disk is reasonable for a recovery simulation lasting several microseconds up to several milliseconds. A number of researchers have simulated the transient heating and cooling of a multi-layered HAMR disk using the continuum Fourier conduction equation [38, 41, 40]. For example, Wu [38, Figures 6(a) and 11(a)] predicted 10 ns cooling time from a disk peak temperature of 440°C to approximately 75°C for a glass substrate and less than 1 ns for the disk to cool from 351°C to 35°C on a more conductive aluminum substrate. In the best experimental evidence of rapid transient disk cooling after laser heating, Ma et al. [20] produced a lubricant depletion track in the shape of

an arc with a 0.9 μm laser spot so the area of current heating usually overlapped with the previous heating. By varying the laser off-time in the pulse laser duty cycle, these researchers concluded that the media temperature is close to room temperature with 40 ns laser off time in one duty cycle because no further change in the magnetic signal image resulted from increasing the off-time.

2.2 Surface Tension

Under HAMR recovery conditions, the surface tension is constant because temperature everywhere is assumed to be ambient. For all simulation studies in this paper, $\gamma = \gamma(T_0) = 23.7$ mN/m. This is in contrast to HAMR writing conditions, where the incident laser results in sharp temperature gradients that induce a surface tension gradient; the surface tension gradient is a major driver of lubricant deformation during HAMR writing [4, 38]. The resultant force of a uniform surface tension acts normal to the interface and is called Laplace pressure or capillary pressure [2]. For quasi-parallel films ($|\nabla h| \ll 1$), force per unit area due to surface tension is $p_{ext} = -\gamma\nabla^2 h$.

2.3 Disjoining Pressure

For sufficiently thin films, the lubricant molecules at the lubricant-air interface experience intermolecular forces from liquid molecules in the film and molecules in the solid substrate. The resultant force per unit area of these interactions is an additional or supplementary pressure acting on an interfacial surface element called disjoining pressure: $p_{ext} = -\Pi$ where Π is the common symbol for disjoining pressure. We use the convention that $\Pi > 0$ means the lubricant-air interface is being repelled from the substrate below. The challenge for accurately predicting lubricant behavior in hard disk drives has been to determine an appropriate model for the disjoining pressure of the particular lubricant-disk system of interest. We will consider two contributions to disjoining pressure and use the mischaracterizing terminology common in hard drive lubricant literature [26]: (1) the *dispersive component* due to van der Waals forces with $1/h^3$ dependence and (2) the oscillating *polar component* that could be due to structural effects or non van der Waals interactions introduced by the functional end-groups. Previous simulations for lubricants covering the disk under HAMR writing conditions have only considered the dispersive component.

The sessile drop method is a widely used technique to determine disjoining pressure of hard drive lubricants from experimental surface energy (contact angle) data. We use the mathematical model for PFPE Zdol from Karis and Tyndall [12] derived using contact angle measurements from their earlier publications [34, 35, 37]. The disjoining pressure is the negative derivative of the free energy gradient with respect to lubricant thickness. Note that surface energy measurements can vary significantly with lubricant end-group, molecular weight, and production or post-production processes such as annealing [34], so by employing this model, we are confining our simulation results to the lubricant-disk systems used in the experimental data to which the disjoining pressure model was fit (unannealed Zdol 2000 coating a production magnetic disk with a 1.3 nm thick amorphous hydrogenated carbon overcoat). We are also limiting our simulations to 0.2 - 2 nm lubricant thickness because that is the limit of the experimental data

on which the disjoining pressure model is based. Other kinds of lubricants will have different intermolecular interactions and therefore need a different disjoining pressure model.

2.4 Viscosity

An explicit formula for viscosity can be derived by applying the method of absolute reaction rates to pure liquids. In this approach, credited to Eyring [30], viscosity and diffusion in a liquid are viewed as rate processes, similar to chemical kinetics. Karis [11] applied Eyring's rate theory to hard disk drive lubricants. The flow activation energy is enhanced by dispersive (van der Waals) forces for thin films.

Figure 2 shows how viscosity varies in our isothermal system at 25°C. Viscosity increases dramatically as the lubricant thins below 1 nm. For the systems we model, the forces are not strong enough to move lubricant in viscous flow below a thickness of about 0.4 nm, so effectively lubricant below this thickness can be considered bonded.

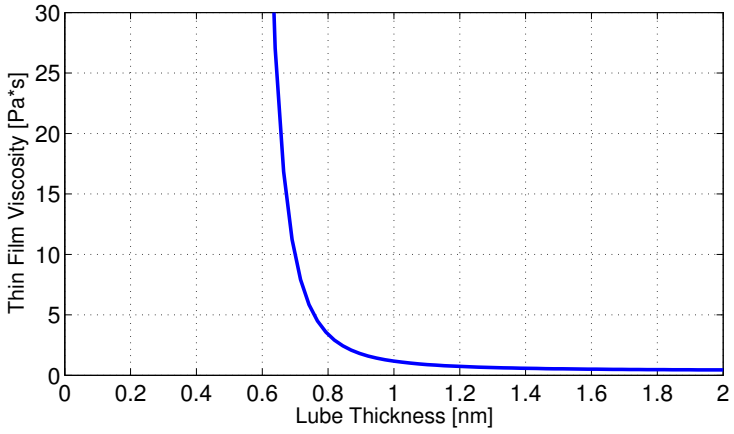

Figure 2: Viscosity model for PFPE Zdol from [11] based on Eyring's rate theory [30] at ambient temperature 25°C during reflow.

2.5 Non-dimensionalized Lubricant System

The lubricant pressure and shear stress can now be determined from the force balance at the lubricant air interface:

$$\begin{aligned} p &= p_{ext} = -\Pi - \gamma \nabla^2 h \\ \tau_x &= \tau_y = 0 \end{aligned}$$

Substituting the determined lubricant pressure and shear stresses into Equation 1, the dimensional governing equation is the following:

$$\frac{\partial h}{\partial t}+\frac{\partial}{\partial x}\left[\frac{h^3}{3\eta}\frac{\partial}{\partial x}\left(\Pi+\gamma\nabla^2 h\right)\right]+\frac{\partial}{\partial y}\left[\frac{h^3}{3\eta}\frac{\partial}{\partial y}\left(\Pi+\gamma\nabla^2 h\right)\right]=0 \tag{2}$$

The obvious non-dimensionalizations are based on system parameters of initial lubricant thickness h_0, initial viscosity $\eta_0=\eta(T_0,h_0)$, and disjoining pressure derivative at the initial lubricant thickness $\frac{d\Pi}{dh}|_{h_0}=\Pi_0'$. We now switch to the notation that quantities with the asterisk subscript are dimensional and the quantities without the asterisk subscript are non-dimensional.

$$h_*=h\,h_0 \qquad \Pi_*'=\Pi'\,\Pi_0' \qquad \eta_*=\eta\,\eta_0 \tag{3}$$

The temporal t_s and length L_s scales are determined in the non-dimensionalization process so that all quantities in the governing equation are of order one and have no coefficient.

$$t_*=t\,t_s \qquad x_*=x\,L_s \qquad y_*=y\,L_s \tag{4}$$

The chain rule is used on disjoining pressure: $\frac{\partial\Pi}{\partial x}=\frac{d\Pi}{dh}\frac{\partial h}{\partial x}$. Substituting Equations 3 and 4 into Equation 2, we determine that the scales and coefficients are as follows:

$$t_s\equiv\frac{3\eta_0\gamma}{h_0^3(\Pi_0')^2} \qquad L_s\equiv\left(\frac{\gamma}{\Pi_0'}\right)^{1/2} \tag{5}$$

The final non-dimensional governing equation for the lubricant flow and evaporation simulations is:

$$\frac{\partial h}{\partial t}+\frac{\partial}{\partial x}\left[\frac{h^3}{\eta}\Pi'\frac{\partial h}{\partial x}+\frac{h^3}{\eta}\frac{\partial}{\partial x}\left(\nabla^2 h\right)\right]+\frac{\partial}{\partial y}\left[\frac{h^3}{\eta}\Pi'\frac{\partial h}{\partial y}+\frac{h^3}{\eta}\frac{\partial}{\partial y}\left(\nabla^2 h\right)\right]=0 \tag{6}$$

The numerical scheme used to solve the non-linear governing equation 6 is based on the simulation code developed by H. Kubotera while he was a visiting scholar at the Computer Mechanics Laboratory [15]. Equation 6 is discretized using the control volume method [28]. First derivatives are approximated by the second-order accurate central difference scheme, and the second derivates in the Laplacian operator are approximated by a fourth-order accurate second derivative finite difference scheme. The code takes advantage of the symmetry in y (cross-track direction, no skew). It is iteratively solved with a Gaussian elimination scheme until the convergence criterion is met. At the edge of the computation domain, the Dirichlet boundary conditions are $h=h_0$.

3 Simulations of Recovery After HAMR Writing

The simulations of lubricant recovery start from a initial profile that is the final profile upon completion of HAMR writing. For HAMR writing, a Gaussian temperature profile with a maximum temperature $T_{max}=350^{\circ}\mathrm{C}$ and varying full-width half maxima

(FWHM) scanned the lubricant surface with speed 5 m/s for a duration of 2 ns [4]. The ambient conditions are $T_0 = 25°C$ and $p_0 = 101325$ Pa = 1 atm. All simulations are for Zdol 2000 with a molecular weight of 2 kg/mol.

We investigate how initial lubricant thickness and the thermal spot size used in HAMR writing effect lubricant recovery. Three thicknesses are considered: 0.7 nm, 1.2 nm, and 1.4 nm. Three thermal spot sizes are considered: (1) 20 nm FWHM, close to the targeted thermal spot size of 25 nm FWHM for 5 Tb/in^2 HAMR recording density [1], (2) 1 μm FWHM, the approximate size of laser spots used in many experimental setups from the literature, and (3) an intermediary size of 100 nm FWHM. In our earlier study [4], writing simulations were preformed for an initial thickness of 0.5 nm, but the deformation was very small, everywhere within 0.1 Å of the initial thickness. So there is no need to perform lubricant recovery simulations for 0.5 nm lubricant because there it is practically undeformed under the simulated writing conditions.

Recovery simulations are run until the lubricant recovers to within 0.1 Å of the initial lubricant thickness, close to the resolution of optical surface analyzers that measure lubricant thickness. Table 1 lists the recovery times for the three thermal spot sizes and the three lubricant thicknesses. We show in an upcoming section that Laplace pressure has a minor effect on lubricant recovery speed and profile shape, so it is neglected for the 20 nm and 100 nm FWHM cases to speed up the computation time. The 20 nm FWHM case had the fastest recover times at all thicknesses: with recovery times in tens of microseconds, the 20 nm FHWM is an order of magnitude faster than the 100 nm FWHM case (hundreds of microseconds) and four orders of magnitude faster than the large 1 μm FWHM case (tens of milliseconds). The 20 nm and 100 nm FWHM cases exhibit the fastest recovery times at 1.2 nm while the 1 μm FWHM case had monotonically increasing recovery time with increasing film thickness. Though the recovery times listed in Table 1 are longer for the largest 1 μm FWHM thermal spot, the interface is quite flat by the next time the slider comes around for a second laser pass. After 15 ms of recovery time, the 0.7 nm lubricant is within 0.107 Å of its initial thickness, the 1.2 nm lubricant within 0.168 Å , and the 1.4 nm lubricant within 0.420 Å .

The lubricant profiles at several times in the recovery process are plotted in Figure 3. To directly compare the lubricant profiles, we normalize the cross-track coordinate by the thermal spot FWHM.

Table 1: Recovery time to within 0.1 Å of initial thickness for various thermal spot sizes (FWHM) and initial thicknesses. Laplace pressure is omitted for the 20 nm and 100 nm FWHM cases to speed up computation time.

Spot Size	0.7 nm	1.2 nm	1.4 nm
20 nm	94.3 μs	10.2 μs	28.2 μs
100 nm	384 μs	256 μs	802 μs
1 μm	17.8 ms	25.5 ms	81.1 ms

The trough recovery rate is a figure of merit for lubricant recovery. The amount of depletion in the trough is greater than the amount of accumulation in the side ridges

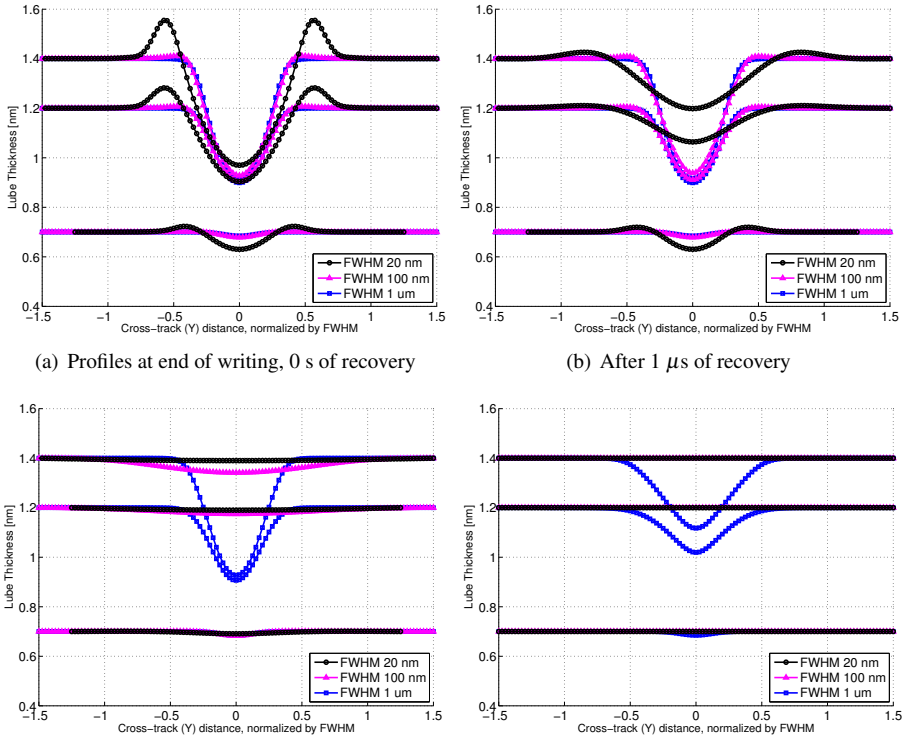

(a) Profiles at end of writing, 0 s of recovery

(b) After 1 μs of recovery

(c) After 100 μs of recovery

(d) After 1 ms of recovery

Figure 3: Cross-track profiles after specified amount of recovery time for different thermal spot sizes used during HAMR writing (illumination time 2 ns, scanning speed 5 m/s, $T_{max} = 350^{\circ}\mathrm{C}$). The cross-track coordinate is normalized by the thermal spot FWHM for direct comparison.

(if present), so the trough is the last to recover and therefore determines recovery time. The trough recovery rate is plotted in Figure 4 is a backward difference approximation of the rate of change of the global minimum point h_{min} between time steps n and $n-1$ separated by length of time Δt:

$$\text{trough recovery rate at time step } n = \frac{h_{min}^{n} - h_{min}^{n-1}}{\Delta t}$$

A maximum exists for the thicker lubricants ($h_0 = 1.2, 1.4$ nm) because other sections of the lubricant profile, the side ridges or another location of the trough, initially have a faster recovery rate due to higher interface slope or higher curvature. Once those features relax, the trough minimum point is the location of fastest recovery, which decreases monotonically in time. The global maximum recovery rate, that is $\min_{i,j}[(h_{i,j}^{n} - h_{i,j}^{n-1})/\Delta t]$, generally decreases in time (not shown). Like a linear spring

restoring force that is proportional to the displacement ($F = -kx$), the restoring disjoining pressure and Laplace pressure forces decrease in magnitude as the lubricant relaxes toward a flat interface. Thus the global recovery rate decreases in time. For all thicknesses, the trough recovery rate of the smallest 20 nm FWHM spot case is an order of magnitude faster than the intermediate 100 nm FWHM case and three orders of magnitude faster than the 1 μm FWHM case. For all thermal spot sizes, the trough recovery rate for 0.7 nm initial thickness is about three orders of magnitude slower than the thicker 1.2 nm and 1.4 nm cases. The tolerance of the algorithm is 10^{-9}, so rates below this value are effectively zero

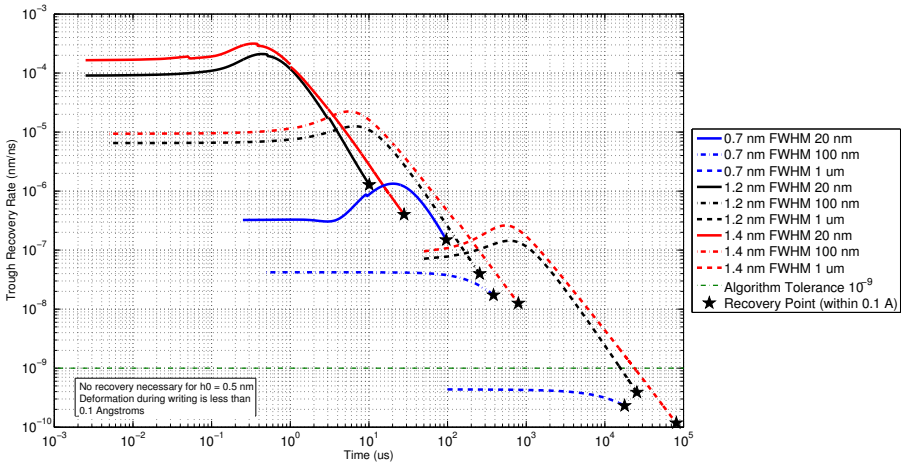

Figure 4: Trough recovery rate for various lubricant thicknesses and thermal spot sizes. A star indicates the time at which the lubricant recovers to within 0.1 Å of the original thickness. The algorithm tolerance is 10^{-9}. Laplace pressure, which has a minor effect on the lubricant profile, is ignored for 20 nm and 100 nm FWHM to expedite the computation time.

Some interesting trends are evident in Table 1 and Figures 3–4: smaller spots recover much faster and an optimal thickness for fastest recovery time exists for smaller spot sizes. Before offering an explanation for these trends, we first discuss the factors that determine lubricant recovery.

3.1 Determinants of Recovery: Driving Forces and Flow Resistance

According to our viscous lubricant model, the driving forces of lubricant recovery are the disjoining pressure and Laplace pressure gradients. Viscosity determines the level of resistance to flow; highly viscous liquids are difficult to drive into flow. Lubricant recovery time depends on the strength of the driving forces and the fluidity (reciprocal of viscosity), or how easily the lubricant flows; stronger driving forces and

higher fluidity/lower resistance to flow lead to faster recovery times. Recasting the non-dimensional governing equation 6, we can group the terms according to contributions to "fluidity" or as a "driving force". Equation 7 is the basis of our explanations and interpretations of our simulations.

$$\frac{\partial h}{\partial t} = \underbrace{-\nabla \cdot \left[\underbrace{\frac{h^3}{\eta}}_{\text{"Fluidity"}} \overbrace{\nabla\left(\Pi + \nabla^2 h\right)}^{\text{"Driving forces"}} \right]}_{\text{Flow = "Fluidity" } \cdot \text{ "Driving forces"}} \tag{7}$$

The driving forces depend on the shape of the lubricant-air interface profile such that severe interface profiles result in faster recovery times. Laplace pressure is a reflection of the mean curvature. The higher the curvature of the interface profiles, the larger the Laplace pressure force and consequently the faster the recovery rate driven by Laplace pressure. Disjoining pressure gradient can be decomposed with the chain rule: $\nabla\Pi = \Pi'\nabla h$ where $\Pi'(h)$ is an explicit function from [12]. Steeper lubricant distortion profiles lead to higher disjoining pressure driving forces and therefore faster recovery times due to the larger values of ∇h.

3.2 Laplace Pressure: A Minor Effect

The lubricant profile and recovery rate are not significantly different if Laplace pressure is excluded. Disjoining pressure is considered to be the main driver of lubricant recovery, and we therefore ignore Laplace pressure if its inclusion leads to very long computation times.

An example of the minor impact of Laplace pressure is illustrated in Figure 5, in which the 20 nm FWHM, $h_0 = 1.2$ nm case is simulated up to 3 μs of recovery with and without Laplace pressure. The impact of excluding the Laplace pressure is minimal as indicated by the minor differences in the trough and side ridge heights. The exclusion of Laplace pressure significantly reduces computation time. To determine the approximate recovery time to within 0.1 Å of the initial thickness, we exclude the Laplace pressure for several cases.

Trough recovery rate and recovery time are also very similar with and without the Laplace pressure. As an example, Figure 6 shows the practically identical trough recovery rate and recovery time to within 0.1 Å of h_0 for the 1 μm FWHM, $h_0 = 1.4$ nm case. The recovery time is 81.1 ms with Laplace pressure and 82.2 ms without Laplace pressure.

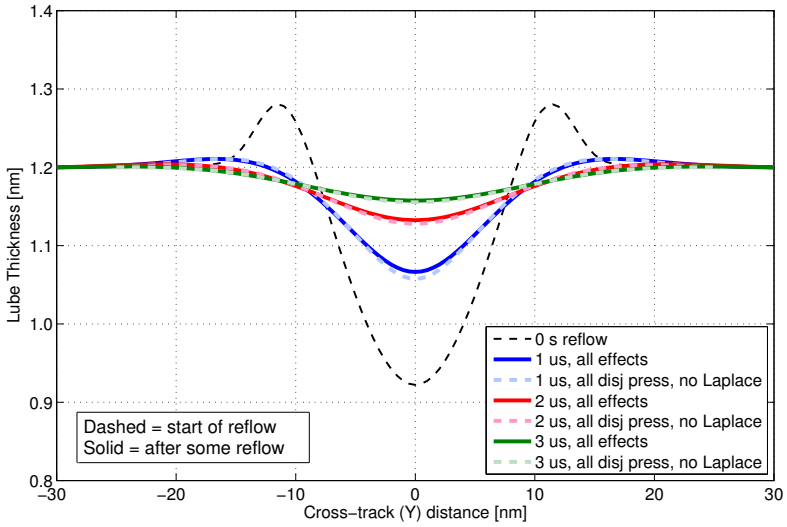

Figure 5: Cross-track lubricant profiles for 20 nm FWHM and initial thickness 1.2 nm with and without Laplace pressure.

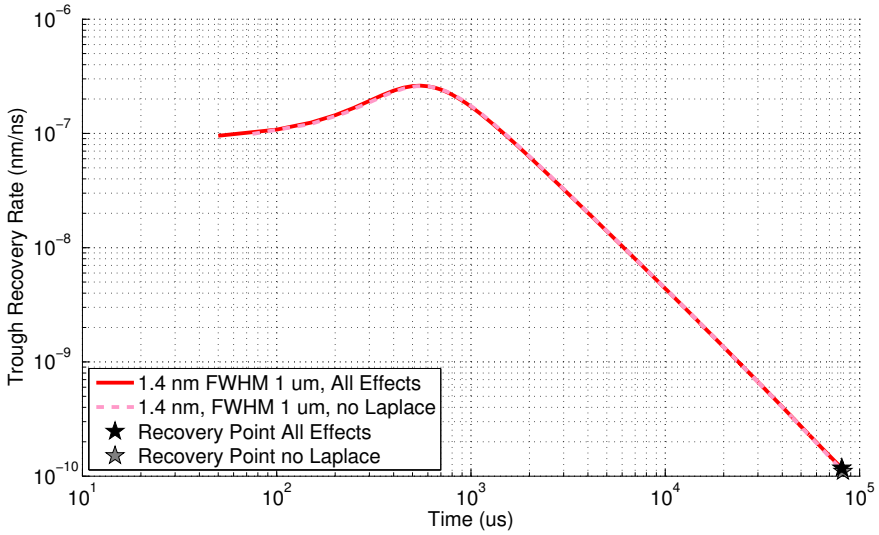

Figure 6: Lubricant trough recovery rates for 1 μm FWHM and initial thickness 1.4 nm with and without Laplace pressure.

3.3 HAMR Lubricant Recovery Trends

Small spots recover faster During writing, we found that the large temperature gradient removed more lubricant due to the fact that thermocapillary shear stress for smaller laser spots form side ridges. Our recovery simulations show that these side ridges add to lubricant deformation and result in faster recovery times. Small spots recover faster because the driving disjoining pressure gradient is much higher due to the sharper profile shape induced by HAMR writing, i.e. ∇h is larger. Inspecting the initial cross-track profiles from Figure 3(a), we see that all three thermal spots have comparable depths in physical units (nm) and comparable trough widths in the FWHM normalized cross-track coordinates for the thicker lubricants of 1.2 nm and 1.4 nm. In other words, Δh is similar but Δy varies proportionally with thermal spot size. The resulting profile shape that determines the recovery rate $\frac{\Delta h}{\Delta y}$ is therefore inversely proportional to the thermal spot FWHM. The driving force for the 20 nm FWHM is initially roughly 5 times larger than the 100 nm FWHM case and approximately 50 times larger than the 1 μm FWHM case. As shown in Figure 4, the trough recovery rate for 20 nm FHWM is much faster than a factor of 5 or 50. The interaction of interdependent terms in the non-linear governing equation and the lubricant profile evolution must also influence this difference in recovery rate.

Thin films recover slower The recovery rate is slower for 0.7 nm initial thickness lubricant systems because the viscosity increases drastically as the lubricant approaches 0.6 nm (Figure 2). In addition, the smaller amount of lubricant deformation for thin systems leads to a smaller ∇h and therefore smaller $\nabla\Pi$ recovery driving force. The high flow resistance (or lower fluidity) and small driving force for the thin lubricants result in slower recovery rates compared to thicker lubricants.

Small spots exhibit an optimal thickness for recovery The amount of recovery needed after HAMR writing can be quantified by performing a discretized integration of the deformation profile. The amount of lubricant above the initial thickness h_0 is accumulation and the amount below h_0 is depletion. The total volume of accumulation and depletion $\Delta h\Delta x\Delta y$ can be normalized for direct comparison of different thermal spot sizes: Δh retains physical units of nanometers and the lateral dimensions $\Delta x, \Delta y$ are normalized by the thermal spot FWHM. The volume to recover following HAMR writing along a cross-sectional slice of width 3·FWHM and the recovery time are plotted in Figure 7. One would expect that as the volume of lubricant depleted and accumulated during HAMR writing increases with increasing lubricant thickness, the time to recover would increase. However, this is a highly non-linear problem with driving forces and fluidity that depend on the solution $h(x,y,t)$. For smaller laser spot systems, the higher ∇h translates to higher restoring $\nabla\Pi$ force that has its fastest recovery rate in a middle thickness range where the lubricant is not too thin to have high viscosity but not too thick so that there is considerable lubricant depletion and accumulation that needs to be recovered. This optimal point becomes more pronounced as the thermal spot size decreases.

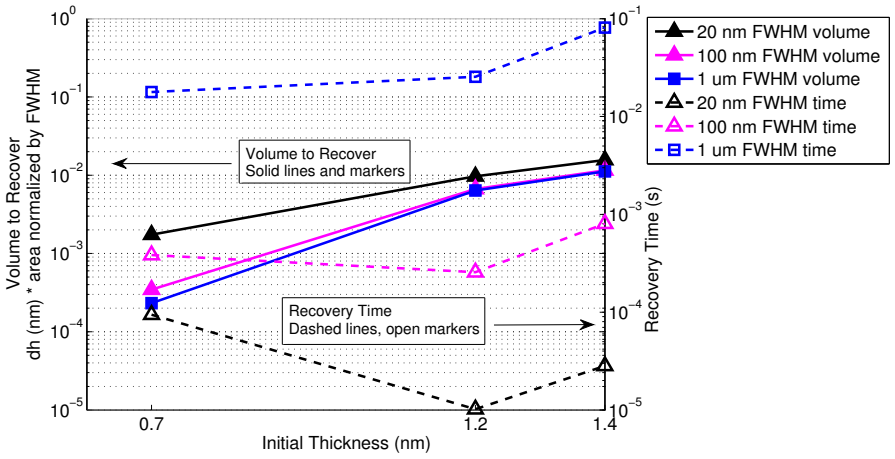

Figure 7: Normalized volume to recover following HAMR writing and recovery time to within 0.1 Å of the initial thickness for different thicknesses and thermal spot sizes. The volume to recover is from a cross-sectional slice 3·FWHM in width.

3.4 Maximum Temperature Study

We have shown that smaller thermal spots recover faster compared to larger spots and argued this is in part due to their "more severe" lubricant deformation. However, the severity of the lubricant depletion can be so catastrophic that the lubricant cannot recover. Table 2 lists the recovery times to within 0.1 Å of the initial 1.2 nm thickness for each maximum temperature. The recoveries of four thermal spot maximum temperature cases is are plotted up to 4 μs in Figure 8. The lower temperature cases recover easily and smoothly from their relatively mild deformations. The 450°C case demonstrates little trough movement after 1 μs but then recovers after this initial resistance. The trough minimum point snaps up once a cone-shaped interface induces a large enough disjoining pressure force between 1 and 4 μs of recovery time (not shown), and the system is able to recover to a flat interface. The trough for the 600°C case does not move in the 4 μs depicted in Figure 8 or in the next 20 μs of simulated recovery. We assume that a crater with vertical sidewalls will remain indefinitely. The difficult recovery behavior after high HAMR writing temperatures is due to high viscosity at the trough minimum thicknesses of 0.4 nm and below.

4 Discussion

We have shown that several Angstroms of lubricant deformation due to 2 ns pulse of a sub-100 nm FWHM thermal spots recover to within 0.1 Å after less than 1 ms. This indicates that the lubricant is well recovered by the second laser pass on a single track under these conditions. Seemingly in contrast, experiments cited in the Section

Table 2: Recovery time to within 0.1 Å of initial thickness for various thermal spot maximum temperatures achieved during HAMR writing. Laplace pressure is neglected to speed up the computation time.

T_{max}	Recovery time
150°C	0.264 μs
300°C	4.73 μs
450°C	34.4 μs
600°C	never

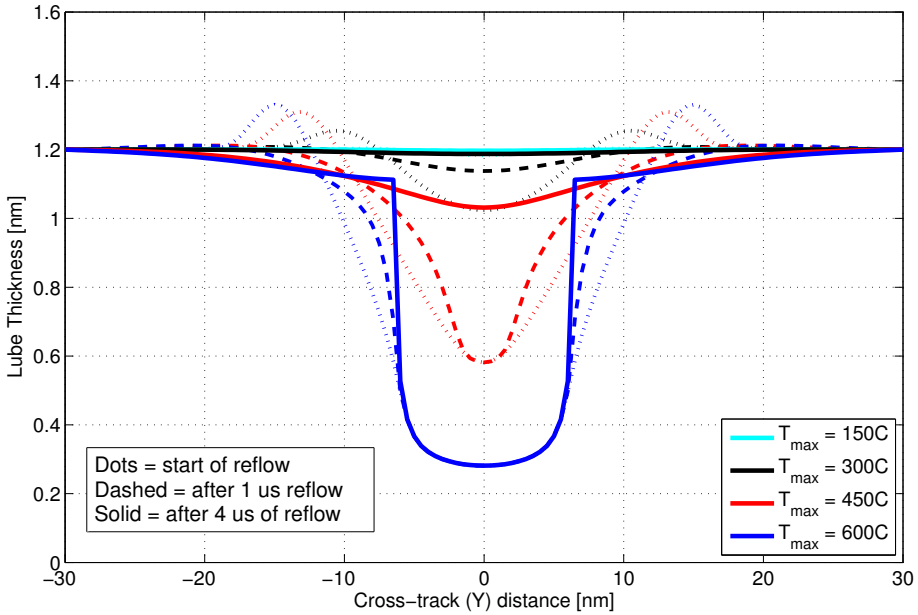

Figure 8: Cross-track lubricant profiles for different maximum temperature achieved during writing with a 20 nm FWHM. Initial (0 s of recovery, immediately after writing) and recovery after 1 μs are shown for each T_{max} case. All effects, including Laplace pressure, are considered. $h_0 = 1.2$ nm, 20 nm FWHM case.

1 demonstrate PFPE lubricants require several hours to recover from laser-induced deformation [21, 20]. However, the severity of the trough profile in [21, 20] is relatively mild, roughly 25 μm in width as measured from the top of the side ridges and 5–10 Å in peak-to-peak variation, leading to a slow recovery process. The driving force is about 1/1250 the magnitude of the same peak-to-peak variation due to a 20 nm FWHM thermal spot. In addition, the Ztetraol is the lubricant test in [21, 20]; the extra two hydroxl end-groups per molecule will increase interaction with the carbon overcoat,

increasing the viscosity and decreasing recovery time.

These recovery studies are for Zdol 2000, a common lubricant in hard drives a decade ago. Modern lubricants such as Ztetraol and ZTMD have more functional end-groups that interact more strongly with the carbon overcoat; therefore the disjoining pressure, viscosity, surface tension, and evaporation (during HAMR writing) models will be different from Zdol property models. Stronger lubricant-carbon overcoat interactions imply that it is more difficult to move and evaporate the lubricant, so the amount of deformation due to thermal spot scanning is expected to be less for a lubricant such as Ztetraol in comparison with the simulation results we present here for Zdol 2000. For future HAMR lubricant writing and recovery studies, we look to add the capability to simulate other lubricant types by incorporating disjoining pressure models for Ztetraol and ZTMD from experimental studies [36, 8]. Suitable experimental data must also be found for the vaporization energy variation with molecular weight for Ztetraol and ZTMD; we expect the vaporization energy will increase linearly with molecular weight as with Zdol, but the constants will differ. In addition, flow activation energy and entropy are properties needed for the viscosity model.

While experimental data for Zdol 2000 under laser illumination is published, validation of our recovery simulation tool is not feasible at this time because lubricant profiles at two specified time points are not given. The simulation tool requires an a initial profile of Zdol 2000 measured at a specified time point as an input, and another profile measured at a later time point is required for the comparison between simulation results and experimental observation. In the literature we have only found such plots for Ztetraol [20]. Once we add the capability to simulate other lubricant types including Ztetraol, we will compare our simulation predictions with the recovery profiles reported in [20].

Because we model the lubricant as a viscous fluid, lubricant recovery occurs more slowly and at a steadier rate than what we expect for actual hard drive lubricants that are known to exhibit viscoelastic behavior. In response to a suddenly applied loading state, such as a sudden application of interface restoring forces upon rapid cooling of the substrate to ambient temperature, a Newtonian viscous fluid responds by a flow process toward equilibrium (flat interface). The rate of recovery depends on the fluid's viscosity. A viscoelastic material will respond with an instantaneous deformation (elastic, solid-like response) followed by a flow process which may or may not be limited in magnitude as time increases (viscous, fluid-like response) [3]. We expect that when we modify our simulation tool to include viscoelastic effects, there will be a rapid elastic response to the restoring forces followed by a slower flow process. The recovery time may or may decrease, depending on the nature of the fluid-like response.

Our model does not account for thermally initiated chemical changes such as cross-linking, cleavage of molecules, or altered nature of the interactions with the carbon overcoat due to changes in the lubricant or the overcoat. Thermal decomposition of bulk Fomblin Zdol occurs at temperatures above 350°C [16, 17], so our high temperature simulations in Section 3.4 should not be interpreted as a quantitative analysis.

5 Conclusion

Interesting and non-obvious results for small HAMR thermal writing spots are predicted by our lubricant recovery simulations. Small thermal spot sizes needed to achieve 5 Tb/in^2 recover on the order to 100–1000 times faster than deformations due to micron-sized optical spots. There appears to be an optimal thickness at which small thermal spot deformations recover fastest, a thickness that is not too thin to have high resistance but not too thick so that substantial lubricant depletion and accumulation needs to be recovered. HAMR lubricant experiments usually are scaled up so that observations can be made using current optical measurement techniques. However, our simulations show that simple scaling of experimental observations using optical laser spots of diameters close to 1 μm to predict phenomena induced by thermal spots close to 20 nm FWHM may not be valid. Researchers should be aware of the possibility of different lubricant behavior at small scales when designing and developing the HAMR HDI.

Acknowledgements

This work was supported by the Computer Mechanics Laboratory at University of California, Berkeley, Mechanical Engineering Department.

References

[1] International Technical Roadmap: Magnetic Data Storage - the technology of magnetic hard disk drives (HDDs). Tech. rep., IDEMA Advanced Storage Technology Committee (ASTC) (2013)

[2] Batchelor, G.: An Introduction to Fluid Dynamics. Cambridge University Press, Cambridge, England (1967)

[3] Christensen, R.M.: Theory of Viscoelasticity, 2nd edn. Academic Press, Inc., New York (1982)

[4] Dahl, J.B., Bogy, D.B.: Lubricant Flow and Evaporation Model for Heat Assisted Magnetic Recording Including Functional End-Group Effects and Thin Film Viscosity. Computer Mechanics Laboratory Blue Report, University of California, Berkeley (2013). Submitted to *Tribology Letters*

[5] Dai, Q., Hendriks, F., Marchon, B.: Washboard effect at head-disk interface. IEEE Transactions on Magnetics **40**(4), 3159–3161 (2004)

[6] Dai, Q., Knigge, B.E., Waltman, R.J., Marchon, B.: Time evolution of lubricant-slider dynamic interactions. IEEE Transactions on Magnetics **39**(5), 2459–2461 (2003)

[7] Dai, Q., Saint-Olive, C., Pit, R., Marchon, B.: Genesis and evolution of lubricant moguls. IEEE Transactions on Magnetics **38**(5), 2111–2113 (2002)

[8] Guo, X., Knigge, B., Marchon, B., Waltman, R.J., Carter, M., Burns, J.: Multidentate functionalized lubricant for ultralow head/disk spacing in a disk drive. Journal of Applied Physics **100**, 044,306 (2006)

[9] Ji, R., Dao, T.K.L., Xu, B.X., Xu, J.W., Goh, B.L., Tan, E., Xie, H.Q., Liew, T.: Lubricant Pickup Under Laser Irradiation. IEEE Transactions on Magnetics **47**(7), 1988–1991 (2011)

[10] Karis, T.: Lubricants for the Disk Drive Industry. In: L. Rudnick (ed.) Lubricant Additives: Chemistry and Applications, chap. 22, pp. 523–584. CRC Press (2009)

[11] Karis, T., Marchon, B., Flores, V., Scarpulla, M.: Lubricant spin-off from magnetic recording disks. Tribology Letters **11**(3-4), 151–159 (2001)

[12] Karis, T., Tyndall, G.: Calculation of spreading profiles for molecularly-thin films from surface energy gradients. Journal of Non-Newtonian Fluid Mechanics **82**, 287–302 (1999)

[13] Karis, T.E., Kim, W., Jhon, M.: Spreading and dewetting in nanoscale lubrication. Tribology Letters **18**(1), 27–41 (2005)

[14] Kryder, M., Gage, E., McDaniel, T., Challener, W., Rottmayer, R., Ju, G., Hsia, Y.T., Erden, M.: Heat Assisted Magnetic Recording. Proceedings of the IEEE **96**(11), 1810–1835 (2008)

[15] Kubotera, H., Bogy, D.: Numerical simulation of molecularly thin lubricant film flow due to the air bearing slider in hard disk drives. Microsystem Technologies **13**(8-10), 859–865 (2007). DOI 10.1007/s00542-006-0275-z

[16] Lei, R., Gellman, A., Jones, P.: Thermal stability of Fomblin Z and Fomblin Zdol thin films on amorphous hydrogenated carbon. Tribology Letters **11**(1), 1–5 (2001)

[17] Li, L., Jones, P., Hsia, Y.T.: Effect of chemical structure and molecular weight on high-temperature stability of some Fomblin Z-type lubricants. Tribology Letters **16**(1-2), 21–27 (2004)

[18] Ma, X., Gui, J., Marchon, B., Jhon, M., Bauer, C.L., Rauch, G.C.: Lubricant replenishment on carbon coated discs. IEEE Transactions on Magnetics **35**(5), 2454–2456 (1999)

[19] Ma, X., Gui, J., Smoliar, L., Grannen, K., Marchon, B., Bauer, C., Jhon, M.: Complex terraced spreading of perfluoropolyalkylether films on carbon surfaces. Physical Review E **59**(1), 722–727 (1999)

[20] Ma, Y., Chen, X., Liu, B.: Experimental Study of Lubricant Depletion in Heat Assisted Magnetic Recording over the Lifetime of the Drive. Tribology Letters **47**(2), 175–182 (2012)

[21] Ma, Y., Chen, X.Y., Zhao, J.M., Yu, S.K., Liu, B., Seet, H.L., Ng, K.K., Hu, J.F., Shi, J.Z.: Experimental Study of Lubricant Depletion in Heat Assisted Magnetic Recording. IEEE Transactions on Magnetics **48**(5), 1813–1818 (2012)

[22] Ma, Y., Gonzaga, L., An, C., Liu, B.: Effect of Laser Heating Duration on Lubricant Depletion in Heat Assisted Magnetic Recording. IEEE Transactions on Magnetics **47**(10), 3445–3448 (2011)

[23] Marchon, B., Saito, Y.: Lubricant Thermodiffusion in Heat Assisted Magnetic Recording. IEEE Transactions on Magnetics **48**(11), 4471–4474 (2012)

[24] Mate, C., Marchon, B.: Shear response of molecularly thin liquid films to an applied air stress. Physical Review Letters **85**(18), 3902–3905 (2000)

[25] Mate, C.M.: Application of disjoining and capillary pressure to liquid lubricant films in magnetic recording. Journal of Applied Physics **72**(7), 3084–3090 (1992)

[26] Mate, C.M.: Taking a Fresh Look at Disjoining Pressure of Lubricants at Slider-Disk Interfaces. IEEE Transactions on Magnetics **47**(1), 124–130 (2011)

[27] Oron, A., Davis, S., Bankoff, S.: Long-scale evolution of thin liquid films. Reviews of Modern Physics **69**(3), 931–980 (1997)

[28] Patankar, S.: Numerical Heat Transfer and Fluid Flow. Hemisphere Publishing Corporation, New York (1980)

[29] Pit, R., Zeng, Q.H., Dai, Q., Marchon, B.: Experimental study of lubricant-slider interactions. IEEE Transactions on Magnetics **39**(2), 740–742 (2003)

[30] Powell, R., Roseveare, W., Eyring, H.: Diffusion, thermal conductivity, and viscous flow of liquids. Industrial and Engineering Chemistry **33**(4), 430–435 (1941)

[31] Rottmayer, R., Batra, S., Buechel, D., Challener, W., Hohlfeld, J., Kubota, Y., Li, L., Lu, B., Mihalcea, C., Mountfield, K., Pelhos, K., Peng, C., Rausch, T., Seigler, M., Weller, D., Yang, X.: Heat-Assisted Magnetic Recording. IEEE Transactions on Magnetics **42**(10), 2417–2421 (2006)

[32] Scarpulla, M., Mate, C., Carter, M.: Air shear driven flow of thin perfluoropolyether polymer films. Journal of Chemical Physics **118**(7), 3368–3375 (2003)

[33] Shukla, N., Gellman, A.J., Gui, J.: The Interaction of CF 3CH 2OH and (CF 3CF 2) 2O with Amorphous Carbon Films. Langmuir **16**(16), 6562–6568 (2000)

[34] Tyndall, G.W., Leezenberg, P., Waltman, R.J., Castenada, J.: Interfacial interactions of perfluoropolyether lubricants with magnetic recording media. Tribology Letters **4**(2), 103–108 (1998)

[35] Tyndall, G.W., Waltman, R.J., Pocker, D.: Concerning the interactions between Zdol perfluoropolyether lubricant and an amorphous-nitrogenated carbon surface. Langmuir **14**, 7527–7536 (1998)

[36] Waltman, R.J.: The interactions between Z-Tetraol perfluoropolyether lubricant and amorphous nitrogenated-and hydrogenated-carbon surfaces and silicon nitride. Journal of Fluorine Chemistry **125**, 391–400 (2004)

[37] Waltman, R.J., Pocker, D., Tyndall, G.W.: Studies on the interactions between ZDOL perfluoropolyether lubricant and the carbon overcoat of rigid magnetic media. Tribology Letters **4**, 267–275 (1998)

[38] Wu, L.: Modelling and simulation of the lubricant depletion process induced by laser heating in heat-assisted magnetic recording system. Nanotechnology **18**, 215,702 (2007)

[39] Wu, L., Talke, F.E.: Modeling laser induced lubricant depletion in heat-assisted-magnetic recording systems using a multiple-layered disk structure. Microsystem Technologies **17**(5-7), 1109–1114 (2011)

[40] Zeng, Y., Zhou, W., Huang, X., Yu, S.: Numerical study on thermal-induced lubricant depletion in laser heat-assisted magnetic recording systems. International Journal of Heat and Mass Transfer **55**(4), 886–896 (2012)

[41] Zhou, W., Zeng, Y., Liu, B., Yu, S., Hua, W., Huang, X.: Evaporation of Polydisperse Perfluoropolyether Lubricants in Heat-Assisted Magnetic Recording. Applied Physics Express **4**, 095,201 (2011)